Optics Letters

Coherent stepped-frequency waveform generation based on recirculating microwave photonic frequency conversion

Cong Ma,[1] Xiangchuan Wang,[1,*] Yue Yang,[1] Zeyong Ding,[1] and Shilong Pan[1,2]

[1]National Key Laboratory of Microwave Photonics, Nanjing University of Aeronautics and Astronautics, Nanjing 210016, China
[2]pans@nuaa.edu.cn
*wangxch@nuaa.edu.cn

Received 19 June 2023; revised 22 August 2023; accepted 6 September 2023; posted 7 September 2023; published 19 September 2023

We propose a novel method for generating coherent and wideband stepped-frequency waveforms using recirculating microwave photonic frequency conversion (MWP-FC). By injecting a narrowband signal into an MWP-FC loop utilizing a dual-parallel Mach–Zehnder modulator (DPMZM), the signal frequency is continuously converted to produce a stepped-frequency waveform with a wide bandwidth. Within the MWP-FC loop, photo-electric conversion is achieved based on self-mixing detection, where the optical phase noise can be suppressed, guaranteeing stability and coherence of the generated signal. In a proof-of-concept experiment, a stepped-frequency signal with a frequency interval of 2 GHz and a bandwidth of about 16 GHz and a stepped-frequency chirp signal with a frequency interval of 3 GHz and a bandwidth of about 15 GHz are generated. In addition, coherence of the generated signals is verified by coherent integration and de-chirping.

https://doi.org/10.1364/OL.498303

Stepped-frequency (SF) waveforms composed of subpulses with different carrier frequencies are widely used in high-resolution radars to reduce the instantaneous bandwidth requirement and improve anti-interference capabilities [1–3]. Modern radars not only employ wide bandwidth signals for high resolution but also demand coherent signals, because their application simplifies the signal processing and improves the signal-to-noise ratio (SNR) [4]. However, conventional electronics hardly meet the requirement of modern radars due to the limited bandwidth. In contrast, microwave photonics exhibits unique features such as the wide bandwidth, low propagation loss, and electromagnetic immunity [5]. Several studies have investigated the SF waveform generation based on different microwave photonic schemes. For instance, an SF waveform generation method based on frequency-to-time mapping (FTM) was proposed in 2010 [6], generating an SF signal with four carrier frequencies at 18, 21.8, 25.6, and 31 GHz but with a small time-bandwidth product (TBWP) of <100. Several schemes based on bias control of an electro-optic modulator were proposed to achieve a larger TBWP [7,8], but the number of the stepped frequencies is restricted due to the limited special bias points. Recently, a photonic digital-to-analog converter (PDAC) based on phase quantization was proposed for reconfigurable radar signal generation [9], where an SF signal with a bandwidth of 4 GHz and a frequency step of 100 MHz is generated. Although the PDAC-based scheme can produce more stepped frequencies, the signal generated by the PDAC has, however, a low SNR due to the small achievable effective number of bits, and the bandwidth is subjected to the bit rate of electronic signal generators (ESGs). To avoid the demand for high-speed ESGs, stepped frequencies can be selected from an optical frequency comb by a thermal tuning silicon microring resonator and converted into a microwave one [10]. Nevertheless, the slow thermal tuning response results in a low switching speed between the stepped frequencies. A solution based on period-one (P1) dynamics of optically injected semiconductor lasers is also proposed to avoid high-speed ESGs but realize fast frequency switching [11]. The major challenge of this solution is the large phase noise due to the instability of P1 dynamics. By using an optoelectronic oscillator, SF signals with the low phase noise can be produced [12]. However, the establishment time of the optoelectronic oscillation and the oscillation bandwidth limit their application. In recent works, optical recirculating frequency shifting and optical heterodyning are combined to generate SF waveforms with an ultra-wide bandwidth [13–15]. The application of the generated signal is successfully demonstrated in radar systems [16,17]. Notwithstanding, it is extremely difficult to produce a stable signal with a pure spectrum as the heterodyne-based method leads to the conversion of the laser phase noise into the electronic domain, severely deteriorating coherence of the signal.

In this Letter, we propose a coherent SF waveform generator based on recirculating microwave photonic frequency conversion (MWP-FC). The system employs a frequency-converted microwave signal as feedback to form an MWP-FC loop. In addition, self-mixing rather than optical heterodyne is employed to achieve photo-electric conversion. A microwave signal is continuously converted in the loop, resulting in a wideband SF waveform. In this process, the conversion of the laser phase noise to microwave phase noise is avoided, thus ensuring stability and coherence of the generated waveform. The proposed solution enables a large stepped-frequency interval with a wide tuning range but without the need to ensure rigorous phased continuity between the frequency-converted signals [18]. In an

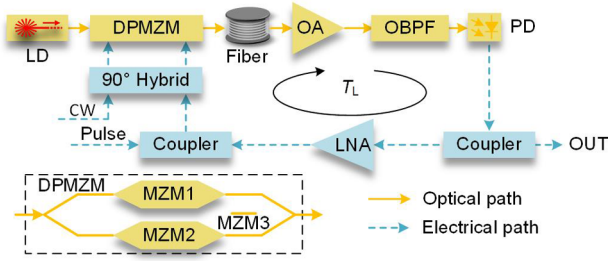

Fig. 1. Schematic of the SF waveform generator. LD, laser diode; MZM, Mach–Zehnder modulator; DPMZM, dual-parallel MZM; OA, optical amplifier; OBPF, optical bandpass filter; PD, photodiode; LNA, low noise amplifier.

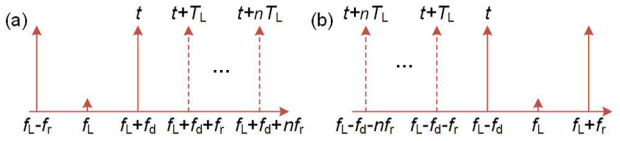

Fig. 2. DPMZM output spectra when the parent MZM is biased at (a) the right quadrature mode or (b) the left quadrature mode.

experiment, an SF waveform generator is established to generate different waveforms including an SF signal and an SF chirp (SFC) signal. The bandwidth of the generated signals is larger than 16 GHz. In addition, coherence of the generated signals is verified by coherent integration and de-chirping.

Figure 1 shows the schematic of the proposed waveform generator, the core of which is an MWP-FC loop consisting of a laser diode (LD), a DPMZM, a 90° hybrid, a fiber spool, an optical amplifier, an optical bandpass filter (OBPF), and a photodiode (PD). A light generated by the LD with a frequency of f_L and frequency noise of $f_N(t)$ is sent to the DPMZM. A reference continuous wave (CW) microwave signal with a frequency of f_r and a driving pulse with a carrier frequency of f_d is fed into the DPMZM via the microwave 90° hybrid. The DPMZM is operated in a single-sideband carrier-suppressed (SSB-CS) modulation mode by biasing the sub-MZMs (MZM1 and MZM2) at the null point and the parent MZM (MZM3) at the quadrature point. When the reference CW and the driving pulse are input to different ports of the 90° hybrid, the DPMZM output spectrum shown by the solid line in Fig. 2 is obtained. When the bias mode of the parent MZM is different (the right or the left quadrature mode), the position of the sidebands is reversed. The output of the DPMZM is expressed as

$$E_{DP}(t) \propto \mathrm{rect}(\frac{t}{T_{pw}}) \cdot \exp\{j[2\pi(f_L \pm f_d)t + \varphi_L(t)]\} + \exp\{j[2\pi(f_L \mp f_r)t + \varphi_L(t)]\}, \quad (1)$$

where $\mathrm{rect}(x)=\{1, |x| \le 0.5; 0, |x| > 0.5\}$, T_{pw} is the pulse width of the driving pulse, and $\varphi_L(t) = 2\pi\int f_N(t)dt$.

Before being sent into the PD, the DPMZM output is sequentially delayed by the fiber spool, amplified by the EDFA, and filtered by the OBPF. The two sidebands excited by the reference CW and the driving pulse experience the same phase fluctuations $\varphi(t-\tau)$, where τ is the microwave photonic link delay. In a PD, the light with two frequency components is converted into a microwave signal by self-mixing. The optical phase noise is canceled out after the optoelectronic conversion, and the

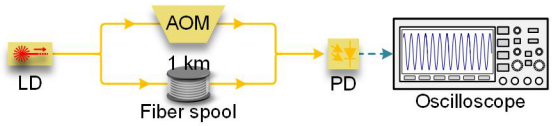

Fig. 3. Experimental setup of the self-heterodyne.

up-converted microwave signal is obtained, written as

$$I(t) \propto \mathrm{rect}(\frac{t}{T_{pw}}) \cdot \cos[2\pi(f_d + f_r) \cdot (t-\tau)]. \quad (2)$$

Thus, the phase of the generated signal based on the proposed system is not affected by the phase noise of the laser, ensuring stability and coherence of the generated signal. This differs from that in Ref. [13–15], where a low-frequency noise laser is required because of the adoption of a heterodyne interferometer.

The PD output is divided into two portions by a microwave coupler. One portion is output to other systems, while the other portion is amplified and fed into the frequency converter. The recirculating frequency conversion will be achieved by adjusting the gain of the loop to compensate for the link loss. Therefore, an SF radar waveform is produced and given by

$$s(t) \propto \sum_{n=1}^{N_{max}} \mathrm{rect}(\frac{t-nT_L}{T_{pw}}) \cos[2\pi(f_d + nf_r)(t-nT_L) + \phi_n], \quad (3)$$

where N_{max} is the maximum frequency conversion number which is limited by the cutoff frequency of the system, T_L is the delay of the frequency conversion loop, and ϕ_n is the initial phase of the nth subpulse. To avoid interference between subpulses, $T_L > T_{pw}$ and $T_r > N_{max}T_L$ have to be satisfied, where T_r is the repetition period of the driving pulse. The system generates an SF signal when f_d is fixed. The frequency f_d can also be time-varying, such as sweeping with time. In this case, an SF chirp signal is generated.

A proof-of-concept experiment is carried out. An LD (Raypro Sensing, RP-FM-10-0080-02) with a frequency of about 194.593 THz is employed in the experiment. To evaluate the performance of the laser, we measure the signal produced from the self-heterodyne interferometer shown in Fig. 3. The laser output is divided into two paths. The upper light propagates through a 200 MHz acousto-optic modulator (AOM, Qingjin G-1550-200), while the lower one is delayed by a 1 km fiber spool. The two signals are coupled into a PD to generate an RF signal with a theoretical frequency of 200 MHz. To analyze stability of the generated signal, we sampled two signals at an interval of 60 μs with a duration of 4 μs. The two parameters, 60 μs and 4 μs, are respectively equal to the signal period and the subpulse duration in subsequent experiments. The spectra obtained at 60 μs intervals are shown by the blue and black curves in Fig. 4. As can be seen, the generated spectrum deviates from 200 MHz when the lower light propagates through the 1 km fiber delay, meaning

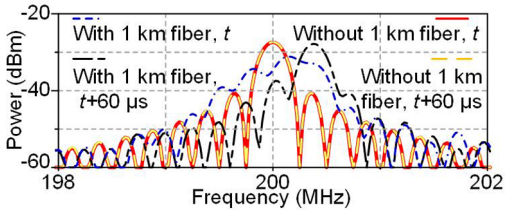

Fig. 4. Spectra of the self-heterodyne output.

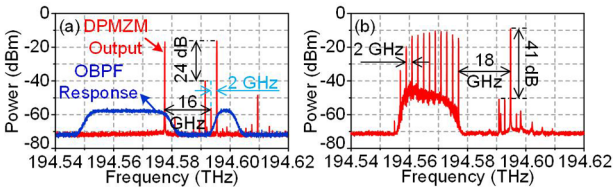

Fig. 5. Output spectrum of (a) the DPMZM and frequency response of the OBPF and (b) the frequency conversion loop.

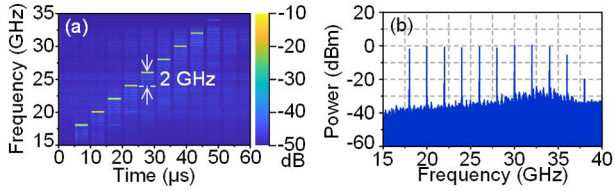

Fig. 6. (a) Time-frequency diagram and (b) spectrum of the SF signal with an incremental frequency of 2 GHz.

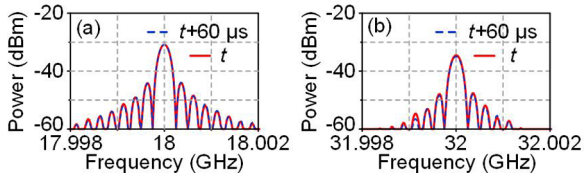

Fig. 7. Spectrum of (a) the first pulse and (b) the eighth pulse of the SF signal with an incremental frequency of 2 GHz.

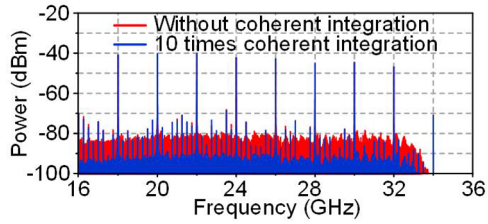

Fig. 8. Comparison of the spectra with 10 times coherent integration and without coherent integration.

that the frequency of the used laser is unstable and impure. For comparison, the spectrum obtained when the lower light does not propagate through the 1 km fiber is also shown by the red and yellow curves. Hence, the scheme proposed in Ref. [13–15] cannot ensure coherence of the generated signal because frequency instability of the laser is converted into microwave ones in the optical heterodyne interferometer.

However, our proposed scheme can completely avoid the impact of laser frequency noise and instability. A signal generation demonstrator is established based on the setup in Fig. 1. The reference CW and the driving pulse signals are respectively generated by a microwave signal generator (Keysight, N5183B) and an arbitrary waveform generator (AWG, Keysight M8195A). First, the frequency of the microwave CW signal is set to 2 GHz, while the frequency, pulse width, and period of the pulse signal are set to 16 GHz, 4 μs, and 60 μs, respectively. The microwave CW and the pulse signal are fed into a DPMZM (Fujitsu, FTM7961) through a microwave 90° hybrid to modulate light from the LD. The modulated light propagates through a fiber spool with a length of about 1 km and enters an erbium-doped fiber amplifier (EDFA, Amonics, AEDFA-PA-35). The loop delay is about 5.17 μs, which is measured by a phase-derived method [19]. Figure 5(a) shows the DPMZM output spectrum when the frequency conversion loop is open. As can be seen, the sideband suppression ratio is only 24 dB although the DPMZM operates in the SSB-CS modulation mode. The low sideband suppression ratio will result in high harmonics in the generating microwave signal. To further suppress the unwanted sidebands, two parallel OBPFs (Yenista, XTM-50) with the frequency response shown by the blue curve in Fig. 5(a) are used. The right passband of the OBPF is set relatively narrow to select the upper sideband excited by the CW signal and suppress the one excited by the pulse signal. The left passband is set relatively wide to select the lower sideband excited by the pulse signal and the feedback signal. The light output from OBPF beats at a PD (Finisar, XPDV2120) with a bandwidth of 40 GHz to generate an upconversion microwave signal, which is amplified by a low noise amplifier (LNA, AT Microwave, AT-LNA-1840-5304 L) and fed into the microwave hybrid through a coupler.

The pump power of the EDFA is adjusted to compensate for the power loss of the frequency conversion loop. The frequency conversion loop outputs the spectrum shown in Fig. 5(b) where more than 9 comb lines are observed. The spectrum shown in Fig. 5(b) indicates that the system achieves cyclic frequency upconversion, resulting in an SF signal. The waveform of the generated SF signal is recorded by an oscilloscope with a sampling rate of 80 GSa/s and an analog bandwidth of 33 GHz. The time-frequency diagram of the SF waveform is shown in Fig. 6(a). The spectrum of the SF signal is also shown in Fig. 6(b). It can be seen that 9 subpulses spanning a frequency range larger than 16 GHz are generated, and the frequency interval between them is 2 GHz. Due to the limited analog bandwidth of the oscilloscope, the power of the high-frequency subpulse is attenuated in Fig. 6(a). To evaluate the suppression effect of laser frequency instability on the system, we used the oscilloscope to acquire waveforms generated at different times and perform the fast Fourier transform (FFT) on them. Figure 7 compares the spectrum at different times of the first and eighth pulses of the SF signal, showing that the frequency of the generated signal is stable.

Due to the existence of electro-optical and photo-electric conversions, the MWP-FC loop has a higher loss compared with the scheme based on the optical recirculating frequency shifting. Therefore, both electrical and optical amplifiers are used in the MWP-FC loop, which may introduce more noise and deteriorate the SNR as the frequency conversion time increases. Fortunately, coherence of the signals produced by the proposed system is preserved because the laser phase noise is eliminated. Therefore, the SNR can be improved by $10\log_{10}N$ dB by using coherent integration, where N is the number of coherent integration [20]. The spectra with 10 times coherent integration and without coherent integration are compared in Fig. 8. As can be seen, the SNR is increased by about 10 dB, verifying coherence of the generated SF signal. It should be noted that the spurs in Fig. 8 are caused by the clock leakage of the oscilloscope rather than the SF signal.

The frequency of the CW and pulse signals driving the DPMZM can be adjusted to enable flexible tunability of the proposed system. By setting the frequency of the CW signal to 3 GHz and changing the pulse driving DPMZM to a chirp signal

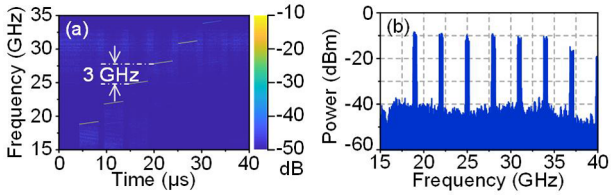

Fig. 9. (a) Time-frequency diagram and (b) spectrum of the SFC signal with an incremental frequency of 3 GHz.

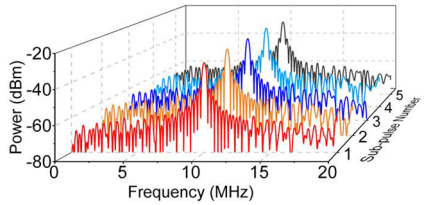

Fig. 10. Spectra of the de-chirped subpulses.

with a center frequency of 16 GHz and a bandwidth of 0.4 GHz, the system can output an SFC signal with an incremental frequency of 3 GHz. Figure 9 shows the time-frequency diagram and spectrum of the generated SFC signal. As can be seen, more than 6 subpulses covering a frequency range of >15 GHz are generated. Due to the limitation of the analog bandwidth of the used oscilloscope, the high-frequency subpulse is not captured, so the time-frequency diagram after the sixth subpulse fails to display in Fig. 9(a).

De-chirping is usually used in SFC signal processing but requires high signal coherence and sufficient frequency sweeping linearity. In the proposed system, the phase jitter of the laser is eliminated to ensure coherence of the generated signal, while frequency sweeping linearity of the generated SFC signal is determined by that of the driving chirp signal with excellent frequency sweeping linearity. Therefore, the generated SFC signal can be processed by de-chirping. We sampled two SFC signals, introduced a 0.1 μs delay between them, and mixed them, resulting in a de-chirped signal. By applying the FFT to the de-chirped waveform, the spectra of the de-chirped subpulses are obtained, as shown in Fig. 10. The mainlobes of the de-chirped spectrum are all located at 10 MHz, which is equal to the theoretical value ($0.1/4\,\mu s \times 400\,MHz = 10\,MHz$). In addition, the mainlobe widths of the de-chirped spectra are consistent with the theoretical value ($0.886 \times 1/(4–0.1\,\mu s) = 0.23\,MHz$), proving excellent linearity and coherence of the produced signal.

In conclusion, we have proposed and experimentally demonstrated coherent SF and SFC signal generations based on an MWP-FC loop. Since the use of self-mixing instead of heterodyne, the produced microwave signal can avoid the effect of the laser phase noise. Thus, coherence of the generated signal is guaranteed. In addition, the proposed system shows features of tunability and wide bandwidth. In the experiment, broadband SF waveforms with a bandwidth of >15 GHz, including an SF signal and an SFC signal, are produced. Moreover, coherence between the generated signals is verified to ensure the radar application.

Funding. National Natural Science Foundation of China (62075095, 62271249).

Disclosures. The authors declare no conflicts of interest.

Data availability. Data underlying the results presented in this paper are not publicly available at this time but may be obtained from the authors upon reasonable request.

REFERENCES

1. M. I. Skolnik, *Radar Handbook*, 3rd ed. (McGraw-Hill, 2008).
2. K. Zhou, D. Li, F. He, S. Quan, and Y. Su, IEEE Trans. Geosci. Remote Sensing **60**, 1 (2022).
3. S. Shao, L. Zhang, and H. Liu, IEEE Trans. Geosci. Remote Sensing **58**, 6791 (2020).
4. S. Maresca, F. Scotti, G. Serafino, L. Lembo, A. Malacarne, F. Falconi, P. Ghelfi, and A. Bogoni, Opt. Lett. **45**, 3953 (2020).
5. J. Yao and J. Capmany, Sci. China Inf. Sci. **65**, 221401 (2022).
6. C. Wang and J. Yao, J. Lightwave Technol. **28**, 1652 (2010).
7. Y. Chen, IEEE Photonics J. **10**, 1 (2018).
8. X. Feng, L. Yan, H. Jiang, P. Li, J. Ye, Y. Zhou, W. Pan, B. Luo, X. Zou, and T. Zhou, IEEE Photonics J. **11**, 1 (2019).
9. J. Li, X. Xue, Z. Xue, B. Yang, M. Wang, and S. Li, Opt. Lett. **47**, 2470 (2022).
10. F. Zhou, X. Wang, S. Yan, X. Hu, Y. Zhang, H. Qiu, X. Xiao, J. Dong, and X. Zhang, IEEE Photonics J. **10**, 1 (2018).
11. P. Zhou, F. Zhang, X. Ye, Q. Guo, and S. Pan, IEEE Photonics J. **8**, 1 (2016).
12. T. Hao, H. Ding, W. Li, N. Zhu, Y. Dai, and M. Li, Photonics Res. **10**, 1280 (2022).
13. Y. Zhang, C. Liu, K. Shao, Z. Li, and S. Pan, Opt. Lett. **45**, 2038 (2020).
14. Y. Lyu, Y. Li, C. Yu, L. Yi, and T. Nagatsuma, J. Lightwave Technol. **40**, 1036 (2022).
15. Z. Zhang, Y. Liu, and B. J. Eggleton, J. Lightwave Technol. **40**, 4521 (2022).
16. C. Ma, Y. Yang, F. Cao, X. Wang, X. Liu, C. Meng, J. Zhang, and S. Pan, IEEE Trans. Geosci. Remote Sensing **60**, 1 (2022).
17. C. Ma, F. Cao, Y. Yang, X. Wang, X. Liu, G. Sun, J. Zhang, J. Fu, and S. Pan, IEEE Trans. Microwave Theory Tech. **71**, 1711 (2023).
18. Z. Yin, X. Zhang, C. Liu, H. Zeng, and W. Li, Opt. Express **29**, 28643 (2021).
19. S. Li, X. Wang, T. Qing, S. Liu, J. Fu, M. Xue, and S. Pan, IEEE Photonics Technol. Lett. **31**, 1351 (2019).
20. J. Zhang, D. Zhu, and G. Zhang, IEEE Trans. Aerosp. Electron. Syst. **49**, 1290 (2013).